Optics Letters

Iridescence-free and narrowband perfect light absorption in critically coupled metal high-index dielectric cavities

M. ElKabbash,[1,*] E. Ilker,[1] T. Letsou,[1] N. Hoffman,[1] A. Yaney,[1] M. Hinczewski,[1] and G. Strangi[1,2,3,4]

[1]Department of Physics, Case Western Reserve University, 10600 Euclid Avenue, Cleveland, Ohio 44106, USA
[2]Case Comprehensive Cancer Center, Case Western Reserve University, Cleveland, Ohio 44106, USA
[3]Department of Physics and CNR-NANOTEC UOS of Cosenza Licryl Laboratory, University of Calabria, 87036 Rende, Italy
[4]e-mail: gxs284@case.edu
*Corresponding author: mke23@case.edu

Perfect light absorption in the visible and near-infrared (NIR) was demonstrated using metamaterials, plasmonic nanostructures, and thin films. Thin film absorbers offer a simple and low-cost design as they can be produced on large areas and without lithography. Light is strongly absorbed in thin film metal-dielectric-metal (MDM) cavities at their resonance frequencies. However, a major drawback of MDM absorbers is their strong resonance iridescence, i.e., angle dependence. Here, we solve the iridescence problem by achieving angle-insensitive narrowband perfect and near-perfect light absorption. In particular, we show analytically that using a high-index dielectric in MDM cavities is sufficient to achieve angle-insensitive cavity resonance. We demonstrate experimentally angle-insensitive perfect and near-perfect absorbers in the NIR and visible regimes up to ±60°. By overcoming the iridescence problem, we open the door for practical applications of MDM absorbers at optical frequencies. © 2017 Optical Society of America

Structural light absorption offers a broad range of possible applications in photonic and optoelectronic devices. In terms of spectral range, light absorbers can be classified as broadband or narrowband absorbers. Broadband light absorbers are useful for applications that rely on efficient light-to-heat generation such as thermo-photovoltaics, thermal emission, and thermal imaging [1]. Narrowband light absorbers are promising candidates for sensing, optoelectronic devices, narrowband selective thermal emission, and structural coloring which can replace traditional colorant pigmentation used in display technologies [2]. Many approaches to achieve structural light absorption require intensive lithography and nanofabrication [3,4] or using plasmonic metasurfaces [5–7]. For more practical applications,

a large-area, lithographically free structural absorber is highly desired. To that end, several works demonstrated broadband absorption using double-layer lossy dielectric-metal films [8] and broad and narrowband absorption using metal-dielectric-metal (MDM) triple layer films [1,9]. The MDM film acts as a subwavelength Fabry–Perot (FP) cavity that resonates with incident light at a given wavelength and angle. While the E field is highly confined inside the dielectric layer due to constructive interference between the incoming and reflected waves, the power is mostly dissipated inside the metallic films [9].

Broadband absorbers are largely insensitive to the incident angle due to their broadband nature which results in a slight change in the absorption intensity at a given wavelength as a function of angle [1]. For narrowband absorbers, however, the angle dependence can be detrimental for practical applications, especially for structural coloring as their color would change significantly [9].

Omnidirectional absorption in MDM cavities was previously proposed, but the proposed system can only operate for a specific cavity thickness and at the surface plasmon frequency of the metal-dielectric interface [10]. Furthermore, the absorption intensity is reduced drastically for larger angles, which would result in effective color angle dependence. In addition, light absorbers based on ultrathin lossy dielectric-metal films cannot produce narrowband absorption due to the high losses in the dielectric film [8]. Depositing an additional metal layer on top of the lossy dielectric can narrow the resonance due to the added interference from the metallic superstrate. However, this is only possible by lowering the losses of the system, e.g., using silicon instead of germanium, and/or the metal used, e.g., using silver instead of gold. Accordingly, such structures are constrained to materials exhibiting strong losses within a given wavelength range, which offers a possible, but limited, solution [11]. Moreover, even after optimizing these structures, the absorption band is of low quality factor ($Q = \lambda/\Delta\lambda \leq 8$), and it does not exhibit perfect absorption because the system is not sufficiently lossy.

In order to realize perfect light absorption, light should be critically coupled to the absorber [12,13]. Critical light coupling takes place when the absorption rate equals the sum of the reflection, transmission, and scattering rates. For an FP cavity, the transmission is blocked by using an opaque bottom metal layer, while scattering is neglected, assuming the thin films are smooth. At resonance, reflection is suppressed due to destructive interference. Conversely, absorption takes place due to losses in the metallic mirrors upon multiple reflections inside the cavity. By optimizing the thickness of the top metal, it is possible to control the finesse and broadness of such critical coupling [9].

In this Letter, we analytically, numerically, and experimentally demonstrate wide-angle range and narrowband perfect absorption in the near-infrared (NIR) and visible regimes in an MDM structure. We show that choosing a dielectric with a high refractive index allows for a wider acceptance angle range, yielding a color preserving structure. It is worth noting that using high-index dielectrics to attenuate iridescence in cavity absorbers was numerically studied in [14]. In addition, Liu *et al.* [15] explained the origin of angle insensitivity in lossy dielectric-metal absorbers based on the high index of refraction for the lossy dielectric used in [8].

To rationalize the design of our system, we first carried out a theoretical analysis of incident angle sensitivity for the reflectance minimum in an MDM thin film structure. The system consists of a top metal layer of thickness t_m, a middle dielectric layer of thickness of t_d, and a bottom metal layer whose thickness is sufficiently large ($\gg$ the skin depth) that it can be considered a semi-infinite substrate. The metal layers have identical composition, with a refractive index n_m and extinction coefficient k_m, while the dielectric is described by a refractive index n_d (the extinction coefficient of the dielectric is assumed negligible in the spectral range of interest). All these quantities are functions of the incident wavelength λ.

For a particular choice of refractive indices and layer thicknesses, we can use the standard transfer matrix approach to numerically solve for the reflectance $R(\theta, \lambda)$ a function of λ and the incident angle θ [16–18]. The numerical results for the wavelength $\lambda_{\min}(\theta)$, where R has a minimum in the NIR regime, are plotted in Fig. 1(a) as dots over a range of θ, for both p- and s-polarized light. Two different systems are illustrated, Ag-MMA-Ag and Ag-Ge-Ag, to show the dramatic contrast between low-index ($n_{\mathrm{MMA}} \sim 1.5$) and high-index ($n_{\mathrm{Ge}} \sim 4.2$) dielectrics used for the middle layer. The bottom Ag layer is assumed to be infinite. The top Ag layer is 22 and 13 nm for the MMA and Ge cavities, respectively. The MMA layer is 560 nm thick, and the Ge layer is 130 nm thick. Clearly, the Ag-MMA-Ag exhibits a much stronger variation $\lambda_{\min}$ with θ than Ag-Ge-Ag. This can be quantitatively seen in Fig. 1(b), which plots $|\lambda_{\min}^{-1} d\lambda_{\min}/d\theta|$; the fractional change in $\lambda_{\min}$ per shift in θ. This quantity is strongly suppressed in the Ge system relative to the MMA one.

To understand the origins of how n_d controls the angular sensitivity of $\lambda_{\min}$, we derive an approximate analytical equation whose solution is $\lambda_{\min}$. To do this, we note that in the transfer matrix approach is the squared amplitude of a complex rational function, $R(\theta, \lambda) = |N_R(\theta, \lambda) + N_I(\theta, \lambda)/D_R(\theta, \lambda) + D_I(\theta, \lambda)|^2$, with N_R, N_I being the real/imaginary parts of the numerator, and analogously for the denominator terms D_R, D_I. When $\sec \theta \sim O(1)$, i.e., for smaller incident angles $\theta \sim 60°$, the minimum in $R(\theta, \lambda)$ as a function of λ coincides with an excellent
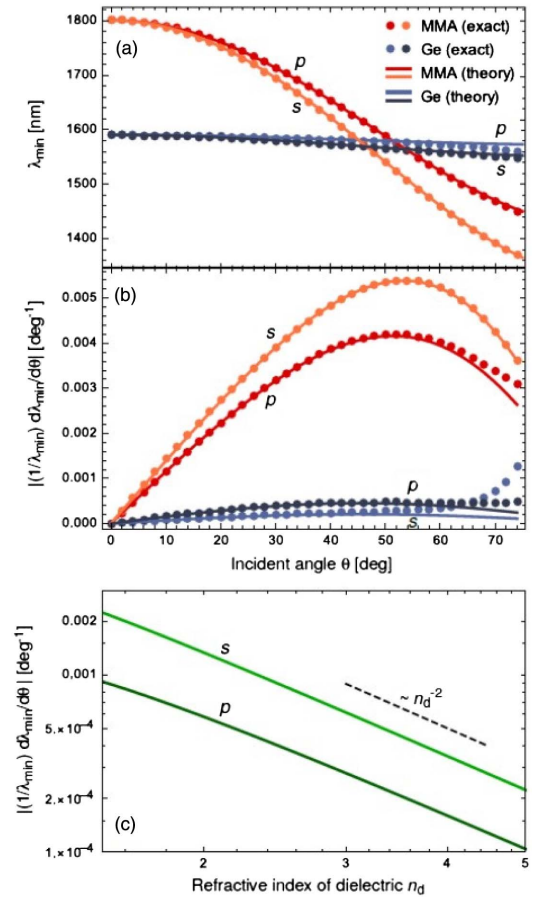
Fig. 1. (a) $\lambda_{\min}(\theta)$ at which reflectance is minimized in the NIR region as a function of the incident angle θ for p- and s-polarized light. The dots correspond to the solution of the exact transfer matrix approach, while the solid lines correspond to the solution of the approximate theory, Eq. (1). Two systems are compared: Ag-MMA-Ag (red/orange) and Ag-Ge-Ag (blue/dark blue). (b) The fractional shift in wavelength per angle, $|\lambda_{\min}^{-1} d\lambda_{\min}/d\theta|$, versus θ for the same systems as in panel (a). (c) Fractional shift per angle versus n_d for an Ag-dielectric-Ag system at $\theta = 20°$, assuming a wavelength independent n_d. The results are calculated using Eq. (1). The t_m and t_d thicknesses here are taken to be the same values as for the Ag-Ge-Ag system in panel (a).

degree of approximation to the point at which $N_I(\theta, \lambda) = 0$. The latter equation has a much simpler analytical form than the condition for the minimum in R, and can be further simplified by assuming $k_m \gg n_m$ and $k_m \gg \sin \theta$, which are valid for Ag in the NIR wavelength range (1300–1800 nm) we are exploring. The end result is an analytical transcendental equation, whose solution for λ at a given θ gives $\lambda_{\min}(\theta)$:

$$\left[\frac{k_m}{n_d} \left(\frac{\alpha_d}{n_d} \right)^{\pm 1} \sinh\left(\frac{2\pi k_m t_m}{\lambda} \right) - \frac{n_d}{k_m} \left(\frac{n_d}{\alpha_d} \right)^{\pm 1} \cosh\left(\frac{2\pi k_m t_m}{\lambda} \right) \right]$$
$$\times \sin\left(\frac{2\pi \alpha_d t_d}{\lambda} \right) + e^{\frac{2\pi k_m t_m}{\lambda}} \cos\left(\frac{2\pi k_m t_m}{\lambda} \right) = 0, \quad \textbf{(1)}$$

where $\alpha_d = \sqrt{n_d^2 - \sin^2 \theta}$. In the terms with ± 1 power, the $+1$ choice corresponds to p-polarization, while the -1 choice corresponds to s-polarization. In the perfect conductor limit,

$k_m \to \infty$, this equation reduces to the conventional relation defining the modes of a dielectric sandwiched between perfectly conducting plates, $\sin(2\pi\alpha_d t_d/\lambda) = 0$, which is the same for p and s. Equation (1) can be seen as a generalization of this mode equation, accounting for the finite values of k_m and t_m, which lead to different mode locations for the two polarizations. The solution $\lambda_{\min}(\theta)$ calculated numerically from Eq. (1) is drawn as a solid line in Fig. 1(a), with the corresponding fractional change per angle in Fig. 1(b). The results have close agreement with the exact transfer matrix approach up to $\theta \approx 60°$, where the $\sec\theta \sim O(1)$ assumption underlying the theory begins to break down. Despite this limitation, the theory provides an accurate representation of most of the angular range covered in our experiments, as we will show later.

Note that α_d is the only term in Eq. (1) that depends directly on the incident angle θ. Though the transcendental equation cannot be solved analytically for $\lambda_{\min}(\theta)$, its structure tells us an important fact. We can use Eq. (1) to derive an implicit differential equation $\lambda_{\min}(\theta)$:

$$\frac{1}{\lambda_{\min}(\theta)}\frac{d\lambda_{\min}(\theta)}{d\theta} = H(\lambda_{\min}(\theta), \alpha_d(\theta))\frac{1}{\alpha_d(\theta)}\frac{d\alpha_d(\theta)}{d\theta}. \quad (2)$$

Here H is a complicated dimensionless function involving the system parameters, but it only depends on θ through $\lambda_{\min}(\theta)$ and $\alpha_d(\theta)$. It is of the order $\sim O(1)$ in our spectral and angular ranges. Thus, the main contributions to setting the magnitude of the fractional change in $\lambda_{\min}(\theta)$ are the terms at the end:

$$\frac{1}{\alpha_d(\theta)}\frac{d\alpha_d(\theta)}{d\theta} = \frac{\cos\theta \sin\theta}{n_d^2 - \sin^2\theta}. \quad (3)$$

As n_d increases to values $\gg 1$, the above expression decreases as n_d^{-2} did. This rapid decrease with the dielectric refractive index is why high-index materials such as Ge show such little fractional change in $\lambda_{\min}(\theta)$. We see the n_d^{-2} scaling directly in Fig. 1(c), which plots $|\lambda_{\min}^{-1}d\lambda_{\min}/d\theta|$ versus n_d for an Ag-dielectric-Ag system at $\theta = 20°$ using $\lambda_{\min}$ solved from Eq. (1). For simplicity, n_d here is assumed independent of wavelength. Both p- and s-polarizations show the same scaling behavior, since they differ only in the form of H. The n^{-2} angular dependence of the fractional change in min in MDM cavities is analogous to that for an all-dielectric cavity [19] which is an interesting analogue that reflects the universality of Eq. (3).

For the design of the NIR perfect absorber, we used an Ag (13.5 nm)-Ge (130 nm)-Ag (70 nm) cavity. Ag was deposited using thermal evaporation, and Ge was deposited using e-beam evaporation. Using a highly reflective metal is essential for narrowband absorption. Individual thin film thicknesses and refractive indices are obtained via spectroscopic ellipsometry (J. A. Woollam, V-Vase). Absorption is considered complementary to reflection in this system since scattering in thin films is negligible and the measured transmission is. Note that the transmission is suppressed in the NIR even for a relatively thin Ag bottom layer since Ag behaves as a nearly perfect electric conductor in the NIR. In order to realize perfect light absorption, our calculations indicated that the Ag top layer should be in the order of 10 nm. Having a very thin Ag film (<20 nm) can be problematic as thin Ag films tend to be irregular and form islands. An irregular Ag film may cause unwanted scattering which can prevent the desired critical light coupling. This is another advantage for using Ge as a dielectric for the NIR

absorber. Very thin Ag films deposited on top of Ge are homogeneous and avoid clustering which further increases light absorption due to reduced surface roughness light scattering [10]. For p-polarized light, we achieved perfect light absorption ($\approx99.8\%$) at 1576 close to the telecommunication wavelength, with a Q-factor of 8 for 65° incidence angle. Figure 2(a) shows the reflectivity spectrum for the Ag-Ge-Ag cavity from 15°–75°. The absorption minimum remains almost unmodified as a function of the incident angle, while the absorption intensity slightly decreases at smaller angles. For comparison, we fabricated an MDM cavity with low n_d dielectric MMA (8.5MMAEL 11, MICROCHEM). The MMA layer was spin-coated at 4000 rpm. Figure 2(b) shows the reflectivity spectrum for an Ag (22 nm)-MMA (560 nm)-Ag (70 nm) cavity. The first-order mode ($m = 1$) of such a cavity coincides spectrally with the Ag-Ge-Ag cavity mode at 45°. We observe considerable spectral shift in the MMA cavity mode for small angular changes. Furthermore, the reflection minimum for the MMA cavity shifts by ≈280 nm for the given angle range compared to only ≈48 nm shift for the Ge cavity, and this is corroborated by the excellent agreement between the experimental and calculated reflectivity data [Figs. 2(c) and 2(d)] [12–14]. The absorption mode of the Ag-MMA-Ag cavity, however, is narrower than that of the Ag-Ge-Ag cavity. This is due to the persistence of non-zero losses for Ge in the NIR which is translated to line broadening of the cavity resonance.

Using germanium as a narrowband absorber in the visible is not possible because it is highly absorbing due to direct electronic transitions at high photon energies [3]. Accordingly, we used titanium dioxide (TiO_2) which has relatively high n' in the visible ($n' \approx 2.2$) and low losses. We fabricated an Ag(30 nm)-TiO_2 (117 nm)-Ag(100 nm). TiO_2 was deposited using e-beam evaporation. The measured and calculated reflectance spectrum for p-polarized light in the visible range from 360 to 750 nm and 15–75 deg is shown in Figs. 3(a) and 3(b), respectively. For the given cavity thickness, we obtained two near-perfect absorption modes ($m = 1$ and 2)
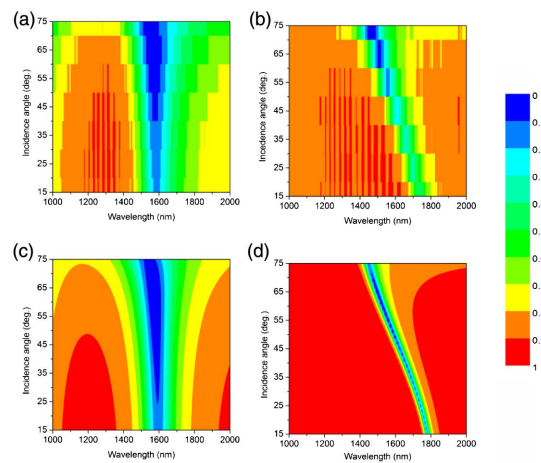
Fig. 2. NIR perfect absorber. (a), (b) Experimental reflectivity spectra for the Ag (13.5 nm)-Ge (130 nm)-Ag (70 nm) and Ag (22 nm)-MMA (560 nm)-Ag(70 nm) NIR absorbers, respectively, for angles of incidence from 15° to 75°. (c), (d) Calculated spectra corresponding to those in (a), (b), respectively. The iridescence of a low-index dielectric (MMA) is clear, compared to the angle insensitivity of high-index dielectric (Ge).
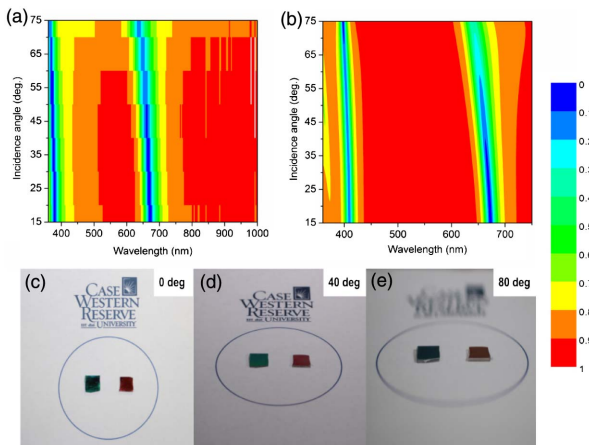
Fig. 3. Visible light absorber. (a), (b) Experimental and calculated reflectivity spectra for Ag(30 nm)-TiO$_2$ (117 nm)-Ag (100 nm) absorber, respectively. Optical images for two wide-angle range visible absorbers are presented in (c), (d), and (e) for 0, 40, and 80 deg, respectively. Clearly, there is no color change for a wide-angle range validating our proposed approach.

reaching ∼94% and 96% absorption and Q-factors of ≈20 and ≈19, respectively, for a 15° incidence angle. Clearly, the modes are highly insensitive to the angle of incidence (see Fig. 3). The shifts in the reflectance minima for $m = 1$ and two modes are ≈33 nm and 18 nm, respectively. The difference between the theory and experiment in the near UV region is due to the use of the Drude model in the theoretical description of the Ag layers. Since this model ignores inter-band transitions, it is known to be a less-than-perfect approximation in the near UV regime where these transitions become relevant.

For applications related to structural coloring, it is important to minimize iridescence for unpolarized light. In our system, the angle insensitivity persists, even for s-polarization. Thus, we have achieved angle-insensitive colors for unpolarized light, representing a relevant technological advantage for many optical applications. To demonstrate the validity of our approach, optical images [Figs. 3(c)–3(e)] were taken for two different Ag(20 nm)-TiO$_2$-Ag(100 nm) films with 90 (green) and 60 nm (pink) thick TiO$_2$ layer at three angles showing no color change. Optical images for low n_d dielectric cavity (SiO$_2$) are presented in the supporting information of Ref. [4] showing different colors at different angles of incidence.

In summary, we demonstrated angle-insensitive narrowband perfect and near-perfect light absorption in the NIR and visible using FP cavities with high-index dielectrics. This Letter provides a practical solution to a major drawback of ultrathin film narrowband absorbers. Here, we relied on critical coupling effects to design and fabricate MDM thin films, which are a low-cost design for perfect absorbers as they can be produced lithographically free on large areas [20]. We demonstrated the angle insensitivity analytically and showed that the fractional change in $\lambda_{\min}$ of minimum reflection as a function of θ scales inversely with the square of the refractive index. In addition, we have fabricated and characterized iridescence-free MDM materials exhibiting narrowband light absorption using an Ag-Ge-Ag cavity in the NIR, and an Ag-TiO$_2$-Ag cavity in the visible. Our system can be used directly in applications related to structural coloring and EM shielding and can act as a reference for designing angle-insensitive light absorbers. In particular, using a high-index dielectric as an overlay on top of any given light absorber should significantly attenuate the absorber angle dependence.

REFERENCES

1. Z. Li, E. Palacios, S. Butun, H. Kocer, and K. Aydin, Sci. Rep. **5**, 15137 (2015).
2. Y.-K. R. Wu, A. E. Hollowell, C. Zhang, and L. J. Guo, Sci. Rep. **3**, 1194 (2013).
3. C. M. Watts, X. Liu, and W. J. Padilla, Adv. Mater. **24**, OP98 (2012).
4. Y. Cui, Y. He, Y. Jin, F. Ding, L. Yang, Y. Ye, S. Zhong, Y. Lin, and S. He, Laser Photon. Rev. **8**, 495 (2014).
5. A. Moreau, C. Ciracì, J. J. Mock, R. T. Hill, Q. Wang, B. J. Wiley, A. Chilkoti, and D. R. Smith, Nature **492**, 86 (2012).
6. G. Liu, Y. Nie, G. Fu, Z. Liu, Y. Liu, L. Tang, and Z. Liu, Nanotechnology **28**, 16 (2017).
7. Z. Liu, X. Liu, S. Huang, P. Pan, J. Chen, G. Liu, and G. Gu, ACS Appl. Mater. Interfaces **7**, 4962 (2015).
8. M. A. Kats, R. Blanchard, P. Genevet, and F. Capasso, Nat. Mater. **12**, 20 (2013).
9. Z. Li, S. Butun, and K. Aydin, ACS Photon. **2**, 183 (2015).
10. H. Shin, M. F. Yanik, S. Fan, R. Zia, and M. Brongersma, Appl. Phys. Lett. **84**, 4421 (2004).
11. K.-T. Lee, S. Seo, J. Y. Lee, and L. J. Guo, Adv. Mater. **26**, 6324 (2014).
12. M. A. Kats and F. Capasso, Laser Photon. Rev. **10**, 699 (2016).
13. V. Romero-García, G. Theocharis, O. Richoux, A. Merkel, V. Tournat, and V. Pagneux, Sci. Rep. **6**, 19519 (2016).
14. J.-B. You, W.-J. Lee, D. Won, and K. Yu, Opt. Express **22**, 7 (2014).
15. D. Liu, H. T. Yu, Y. Y. Duan, Q. Li, and Y. M. Xuan, Sci. Rep. **6**, 32515 (2016).
16. V. J. Logeeswaran, N. P. Kobayashi, M. S. Islam, W. Wu, P. Chaturvedi, N. X. Fang, S. Y. Wang, and R. S. Williams, Nano Lett. **9**, 178 (2009).
17. A. R. Forouhi and I. Bloomer, Phys. Rev. B **38**, 1865 (1988).
18. U. Y. Honghua, J. D'Archangel, M. L. Sundheimer, and E. Tucker, Phys. Rev. B **91**, 235137 (2015).
19. V. R. Shrestha, S.-S. Lee, E.-S. Kim, and D.-Y. Choi, Sci. Rep. **4**, 4921 (2014).
20. J. R. Fan, W. G. Wu, Z. J. Chen, J. Zhuab, and J. Li, Nanoscale **9**, 3416 (2017).